

# Stand-off mapping of the soot extinction coefficient in a refinery flare using a 3-wavelength elastic backscatter LIDAR

Renata F da Costa<sup>a</sup>, Riad Bourayou<sup>a</sup>, Eduardo Landulfo<sup>a</sup>, Roberto Guardani<sup>b</sup>, Igor Veselovskii<sup>c</sup> and Juliana Steffens<sup>d</sup>

<sup>a</sup>Instituto de Pesquisas Energéticas e Nucleares, Avenida Prof. Lineu Prestes 2242, São Paulo, 05508-000, Brazil;

<sup>b</sup>Escola Politécnica da Universidade de São Paulo, Avenida Gualberto 2345, São Paulo, 05508-970, Brazil;

<sup>c</sup>Physics Instrumentation Center, A.M. Prokhorov General Physics Institute, Russian Academy of Sciences, 38 Vavilov Str., 119991 Moscow, Russia;

<sup>d</sup>Regional Integrated University of Upper Uruguai and Missions, Department of Food Engineering, URI Erechim, Av. Sete de Setembro, 1621, Erechim, 99700-000, Brazil.

## ABSTRACT

In this study, a mapping of the soot extinction coefficient in an oil refinery flare using a three-wavelength elastic backscatter lidar system is presented. A log-normal aerosol size distribution was assumed for the flare, and a homogenous refractive index was assumed along the nearly horizontal beam path through the atmosphere, excluding the flare volume. The optical depth was estimated for each wavelength and from this the Angström exponent was calculated. The results were comparable with the literature, demonstrating that it is possible to distinguish small from large particles by this technique in low wind conditions.

**Keywords:** Lidar system, Extinction coefficient, Petrochemical flare, Aerosol monitoring, Angström exponent

## 1. INTRODUCTION

Characterization of atmospheric emissions from industrial flare stacks represents a measurement challenge because it is difficult to determine the real-time concentrations of combustion products by in situ sampling. Stack access constraints, sensor calibration problems, and emission pattern fluctuations limit the practicality of this approach.

Optical remote sensing techniques have significant advantages for gas and particle pollutant detection over conventional systems, which are usually based on sampling and measurement by a train of analytical devices.<sup>1</sup> Remote optical methods offer three important advantages: on-line evaluation of the measurement, no contamination of samples and the capability of scanning large areas. Optical remote sensing devices based on the lidar (light detection and ranging) technique are relatively simple in construction, and can detect changes in optical response in real time over large distances, probing hostile environments where fluctuations of temperature and pressure can be large. These features enable the technique to be applied to monitoring of industrial emissions with rapidly varying physical-chemical composition.

While aerosols in flames have been studied through in situ and optical methods in the laboratory,<sup>2-4</sup> to the authors' knowledge lidar-based field measurements of aerosol properties of industrial flames have not been reported in the literature. In this study it is shown that by assuming horizontal homogeneity for the atmosphere and a particle size distribution function during measurements, it is possible to map the optical depth and Angström exponent across the flame using near-horizontal multiwavelength elastic backscatter lidar measurements.

---

Further author information: (Send correspondence to Renata F da Costa)  
Renata F da Costa: E-mail: renata.facundes.costa@usp.br, Telephone: +55 (11) 3133 9255

## 2. SYSTEM SETUP

The study presented here was carried out in the industrial area of the city of Cubatão ( $23^{\circ} 53' S / 46^{\circ} 25' W$ ), in the Southeast of Brazil, located on the Atlantic coast about 50 km from São Paulo, one of the largest industrial sites in the country. The lidar system was installed approximately 400 m from one of the industrial flare stacks, which has a total height of approximately 40 m and diameter of 2 m. The stack location relative to the lidar was roughly 30 degrees east from the geographical north.<sup>5</sup>

The commercially-produced Raymetrics lidar system employed is a three-wavelength elastic backscatter system operating in the biaxial mode. The light source is a Nd:YAG laser (CFR 450, Quantel S.A.) operating at 355 nm, 532 nm, and 1064 nm, transmitting pulses of  $7 \pm 2$  ns in duration at a fixed repetition rate of 20 Hz. The emitted laser pulses have a divergence of less than 0.3 mrad. The receiver used to collect the backscattered laser light is a 150 mm diameter Dall-Kirkham telescope with an effective focal length of 1000 mm. The lidar is currently operated with a fixed field of view (FOV) of 1 mrad, which permits a full overlap between the telescope FOV and the transmitted laser beam at a range of approximately 140 m from the lidar system. A 20 MHz sampling rate of the detection electronics gives a range resolution of 7.5 m. The instrument was found to be sensitive to backscatter from distances up to 7 km.

The backscattered laser radiation is detected by two photomultiplier tubes (Hamamatsu) and one Si-avalanche photodiode (EG&G) coupled to narrowband interference filters to assure the reduction of the solar background during daytime operation and to improve the signal-to-noise ratio (SNR). The PMT output signal is recorded by a Transient Recorder (Licel) in both analog and photon counting modes.

The laser and telescope are attached to a scanning base adapted from a 2 AP sun tracker (Kipp&Zonen) that performs changes in both azimuthal and polar angles with an accuracy of less than 0.02 degrees. This system has two stepper motors controlled by an on-board microcomputer to allow full scanning over a desired angle range.

## 3. METHODOLOGY

A 12 x 12 virtual matrix was used to divide the flare region into cells as shown (not to scale) in Fig. 1. Starting from the lower left cell the lidar scan was conducted to the right, up, to the left, and so on, thus forming a zigzag pattern until the last cell. The variations of the zenithal and azimuthal angles were made in steps of 0.02 and 0.03 degrees, respectively. During the acquisition for each cell of the matrix, the integration time was fixed to 10 seconds. All data were collected in a period of approximately 40 minutes.

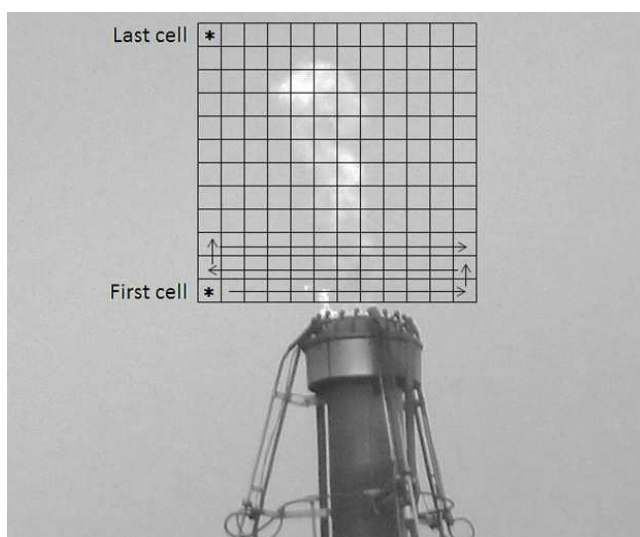


Figure 1. View of the top of the flare stack with the data collection grid [arrows indicate measuring sequence].

### 3.1 Data analysis

In order to calculate the optical depth and Angström exponent from the multiwavelength lidar measurements the following assumptions were made:

- the backscattering coefficient was considered constant along the lidar measurement path since a low zenithal angle was used for acquisition through an atmosphere that was assumed to be horizontally homogeneous;
- the aerosol size distribution in the flame was considered log-normal;
- the refractive index of the particles was considered constant throughout the flame;
- multiple scattering effects were assumed to be negligible.

These assumptions are in accordance with the literature,<sup>1,6</sup> except for the third one, which requires additional study because it is known that the refractive index is temperature dependent and thus in reality varies somewhat across the flame.<sup>7</sup> The validity of this assumption is discussed in the results section. The optical depth of the flame was determined from the drop in received range-corrected signal across the flame as follows. The range-corrected signal,  $S(r, \lambda)$ , is expressed as

$$S(r, \lambda) = C\beta(\lambda) \exp \left[ -2 \int_{r_0}^r \alpha(r', \lambda) dr' \right], \quad (1)$$

where  $\beta(\lambda)$  is the backscattering coefficient, which in this case depends only on the wavelength, and  $C$  is the system factor which contains all the geometrical and system parameters such that

$$C = P_0(\lambda) \frac{c\tau}{2} A\eta O(r'). \quad (2)$$

Here  $P_0(\lambda)$  is the laser power,  $c$  is the speed of light,  $\tau$  is the pulse length in seconds,  $A$  is the effective area of the telescope,  $\eta$  is the optical efficiency and  $O(r')$  is the overlap function after reference range,  $r'$ , where it reaches unity. The optical depth  $\gamma(r)$  can be expressed as

$$\gamma(r) = \int_{r_0}^r \alpha(r', \lambda) dr', \quad (3)$$

where  $\alpha(r', \lambda)$  is the extinction coefficient. By choosing two distinct points from the data, one before the flame, at  $r_1$ , and another one after the flame, at  $r_2$ , the following expression can be written:

$$\frac{S(r_1, \lambda)}{S(r_2, \lambda)} = \frac{C\beta(\lambda) \exp[-2\gamma(r_1)]}{C\beta(\lambda) \exp[-2\gamma(r_2)]} = \exp\{-2[\gamma(r_1) - \gamma(r_2)]\} = \exp[-2\gamma_f], \quad (4)$$

where  $\gamma(r_1)$  is the optical depth up to the leading edge of the flame, and  $\gamma(r_2)$  is the optical depth up to the trailing edge of the flame. The optical depth of the flame  $\gamma_f$  can then be expressed as

$$\gamma_f(\lambda) = -\frac{\ln[S(r_1, \lambda)/S(r_2, \lambda)]}{2}. \quad (5)$$

The Angström exponent  $k$  can be retrieved from the optical depth estimated at two different wavelengths,  $\lambda_1$  and  $\lambda_2$ :

$$k = -\frac{\ln[\gamma_f(\lambda_1)/\gamma_f(\lambda_2)]}{\ln[\lambda_1/\lambda_2]}. \quad (6)$$

## 4. RESULTS

Figure 2 shows the intensity of the range-corrected backscattering lidar signal (Eq. 1) around the stack flame at 355 nm, 532 nm and 1064 nm respectively, in arbitrary units. The wind speed was low during the monitoring campaign, below the threshold of the sodar used to monitor it, so the flame could be considered stable throughout the measurements.

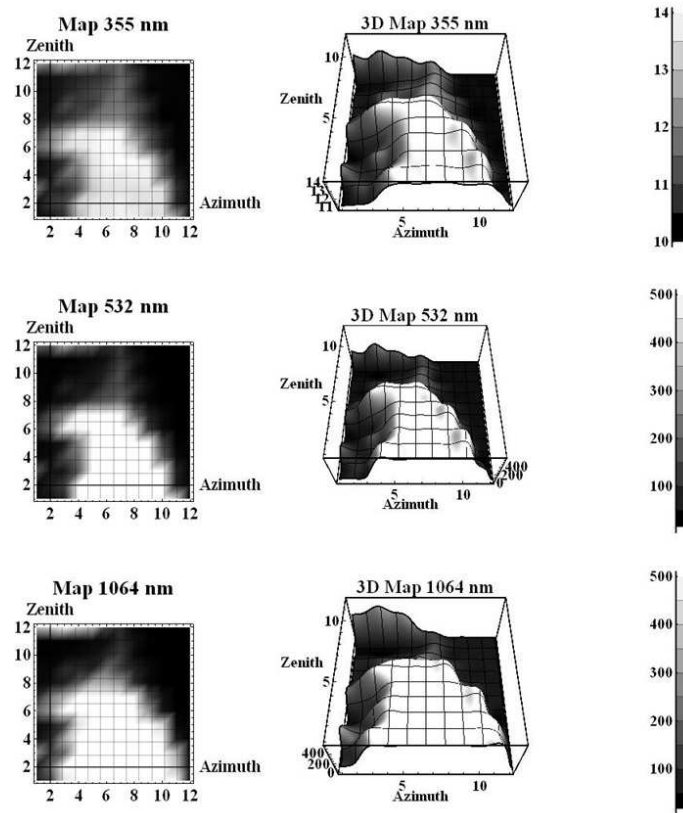


Figure 2. Range-corrected scanning lidar return signal from the flare at 3 wavelengths.

Figure 3 shows the optical depth distribution across the flame for each of the three wavelengths. At 1064 nm the optical depth is highest in a ring around the center of the flame base. According to the literature, higher concentrations of soot particles are expected in this region in stable flames.<sup>4</sup> At 532 nm and 355 nm, the optical depth is largest at the center of the flame base. In this region the difference between the 1064 nm optical depths and those of the other two wavelengths suggests that particles are very small in this region, and exhibit Rayleigh extinction. In a sensitivity test, the uncertainties in the results varied between 18 and 20%, being larger to the measures at the bottom of the flame and the smaller at the top.

Figure 4 shows the Angström exponent for wavelength ratios of 1064/355 and 1064/532. This figure shows that the values in the bottom of the flame are larger than those in the top. If a similar size distribution function is assumed throughout the flame, in a first interpretation the Angström exponents indicate that the particles in the bottom are smaller than those in the top. Studies show, although, that variations in complex refractive index make it more difficult to draw conclusions about the particle sizes from the Angström exponent alone.<sup>8</sup> However, these results can be used to define the homogeneous regions of the complex refractive index, which will be necessary to know to retrieve later the particle size distribution.

According to the literature, it is possible to set the refractive index of the particles along the flame.<sup>9,10</sup> These works show that refractive index distribution is dominantly influenced by the temperature in the flame, and on

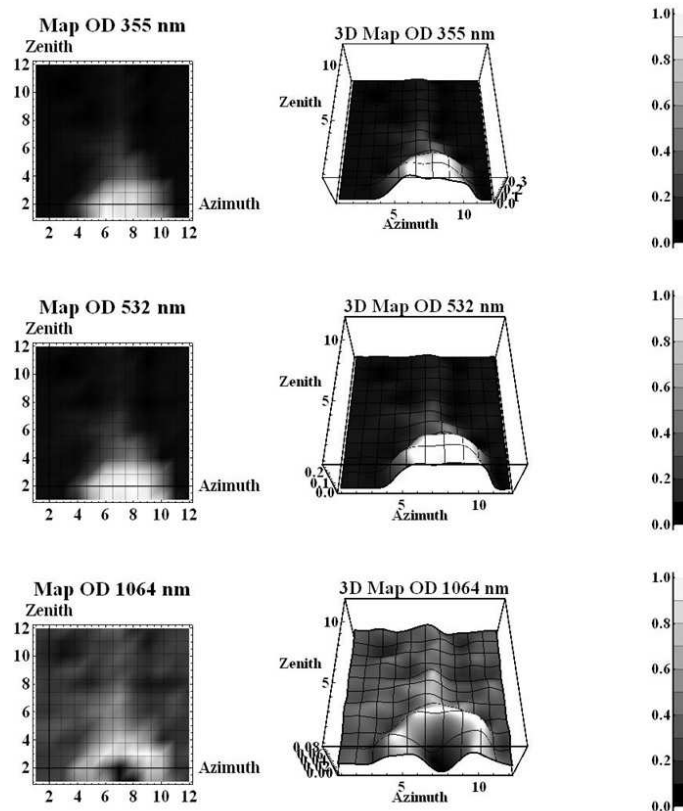


Figure 3. Flare optical depth distributions.

the lean or rich side of stoichiometric mixture ratio the refractive index is directly related to the progress of turbulent mixing and of the reaction process.

## 5. CONCLUSION

The results of the monitoring campaign with the lidar directed to the flare stack tip, though preliminary, indicate that it is possible to gather information about particle sizes in flames using elastic-only multiwavelength lidar. This evidence brings new perspectives for further studies on retrieval methods that could provide information on particle size properties of atmospheric emissions from stacks. This can lead to the development of remote monitoring techniques based on lidar applied to industrial flares, which can represent an attractive alternative to monitor atmospheric emissions in industrial facilities, thus helping companies improve the efficiency and compliance of their processes.

## ACKNOWLEDGMENTS

The authors would like to thank the Brazilian research support agencies FAPESP (2011/00769-7, 2012/00539-4, 2012/00809-1, 2012/19052-8 and 2013/01301-4), CNPq and CAPES for the financial support, as well as CEPEMA (Environmental Research Center of the University of Sao Paulo) and Petrobras for the technical support and motivation. The first author also would like to thank Dr. Joshua Vande Hey for the valuable discussions and great help in structuring and correcting of the text.

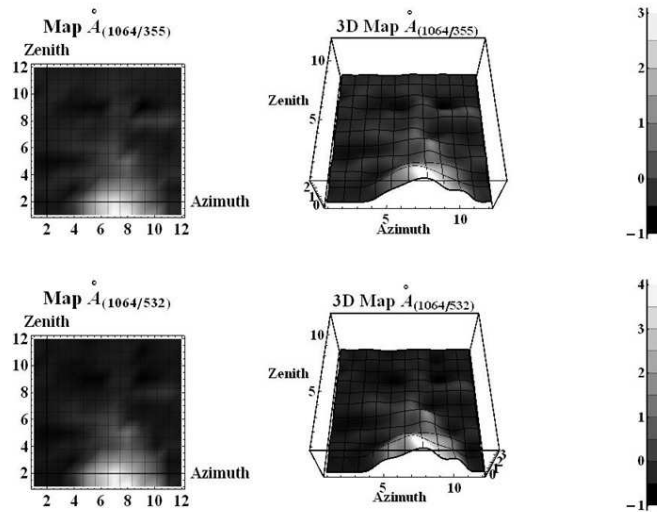


Figure 4. Angström exponent distribution over the measuring grid at the flare.

## REFERENCES

- [1] Eichinger, W. E. and Kovalev, V. A., [*Elastic Lidar: Theory, Practice, and Analysis Methods*], Wiley Publishers (2004).
- [2] Weibring, P., Andersson, M., Edner, H., and Svanberg, S., "Remote monitoring of industrial emissions by combination of lidar and plume velocity measurements," *Applied Physics B: Lasers and Optics* **B66**(3), 383–388 (1998).
- [3] Duwig, C., Li, B., Li, Z., and Aldén, M., "High resolution imaging of flameless and distributed turbulent combustion," *Combustion and Flame* **159**(1), 306–316 (2012).
- [4] Hall, R. J. and Bonczyk, P. A., "Sooting flame thermometry using emission/absorption tomography," *Appl. Opt.* **29**(31), 4590–4598 (1990).
- [5] da Costa, R. F., Landulfo, E., Nakaema, W. M., Bourayou, R., Junior, P. F. M., and Guardani, R., "Preliminary studies of the backscattering of industrial flare using lidar technique in cubatao, brazil.," in [*Proceedings of 26th ILRC*], (2010).
- [6] Netzell, K., Lehtiniemi, H., and Mauss, F., "Calculating the soot particle size distribution function in turbulent diffusion flames using a sectional method," *Proceedings of the Combustion Institute* **31**, 667–674 (2007).
- [7] Kharitonov, A. I., Khoroshko, K. S., and Shkadova, V. P., "Temperature dependence of air refraction at high temperatures," *Fluid Dynamics* **9**, 851–853 (1974).
- [8] Jung, C. H. and Kim, Y. P., "Analytic solution on the estimation of the angstrom exponent in log-normal aerosol size distribution," *Particulate Science and Technology* **31**(1), 92–99 (2013).
- [9] Habib, Z. G. and Vervisch, P., "On the refractive index of soot at flame temperature," *Combustion Science and Technology* **59**(4-6), 261–274 (1988).
- [10] Davis, M. R., "Turbulent refractive index fluctuations in a hydrogen diffusion flame," *Combustion Science and Technology* **64**(1-3), 51–65 (1989).